Quantitative model of diffuse speckle contrast analysis for flow measurement

Jialin Liu
Hongchao Zhang
Jian Lu
Xiaowu Ni
Zhonghua Shen

SPIE.

Quantitative model of diffuse speckle contrast analysis for flow measurement

Jialin Liu, Hongchao Zhang, Jian Lu, Xiaowu Ni, and Zhonghua Shen*
Nanjing University of Science and Technology, School of Science, Nanjing, China

Abstract. Diffuse speckle contrast analysis (DSCA) is a noninvasive optical technique capable of monitoring deep tissue blood flow. However, a detailed study of the speckle contrast model for DSCA has yet to be presented. We deduced the theoretical relationship between speckle contrast and exposure time and further simplified it to a linear approximation model. The feasibility of this linear model was validated by the liquid phantoms which demonstrated that the slope of this linear approximation was able to rapidly determine the Brownian diffusion coefficient of the turbid media at multiple distances using multiexposure speckle imaging. Furthermore, we have theoretically quantified the influence of optical property on the measurements of the Brownian diffusion coefficient which was a consequence of the fact that the slope of this linear approximation was demonstrated to be equal to the inverse of correlation time of the speckle. © *2017 Society of Photo-Optical Instrumentation Engineers (SPIE)* [DOI: 10 .1117/1.JBO.22.7.076016]

1 Introduction

Laser speckle contrast imaging (LSCI)[1–4] has emerged as a powerful technique for visualizing blood flow *in vivo*[5–8] with high temporal and spatial resolution. LSCI is performed by the illumination of the biological tissue with a coherent light source and imaging of the reflected laser speckle with a camera. The motion of the scattering particles results in blurring the speckle within a finite integration time. The extent of this localized spatial blurring is defined as the speckle contrast K, by calculating the ratio of the standard deviation (σ_s) to the mean intensity ($\langle I \rangle$) within a local region[9] in the speckle image, i.e., $K = \sigma_s / \langle I \rangle$.

Traditionally, under the condition of single scattering, the models[10] relating speckle contrast to exposure time are used to extract blood flow information from the speckle contrast measurements by calculating the correlation time of the speckle. From dynamic light scattering (DLC)[11] theory, this correlation time is shown to be inversely proportional to the speed of the scattering particles.[12] Therefore, accurate estimation of correlation time is especially important for quantitative flow measurement. Many researchers[13–16] attempt to improve the instrumentation and theory of LSCI to extract reliable measurement of correlation time from the speckle contrast. For example, Parthasarathy et al.[15] presented multiexposure speckle imaging (MESI) to consider the effect of static scattering on the measurement of correlation time and further to improve computational accuracy of correlation time in flow phantom and *in vivo*.[17,18]

The primary limitation of LSCI is that it requires some assumptions regarding single scattering and the form of the velocity distribution (Lorentzian or Gaussian distribution)[19] for estimating the correlation time. In fact in a larger diameter vessel, where photons may experience multiple scattering[20,21] events before arriving at the camera, the scattering angle information and the polarization of scattered light are lost, and the single scattering model breaks down. In this case, the technique of diffuse correlation spectroscopy (DCS)[22,23] can be applied further for characterizing the dynamic properties of multiple scattering media. The capability of DCS for measuring the motion of the scattering particles depends on the measured temporal autocorrelation function of the back-scattered speckle patterns. Furthermore, some studies[24,25] showed that the combination of DCS and LSCI, i.e., diffuse speckle contrast analysis (DSCA), held potential for measuring the flow change in the deep tissue. They used the linear relation between $1/K^2$ and dynamic parameters to consider $1/K^2$ as an index of blood flow. Similar to LSCI, it has been demonstrated that DSCA has the advantage of simplifying the instrument in hardware and computation process. However, unlike DCS, they did not directly use a model to separate the effects of tissue geometry, source–detector (SD) separation, and the baseline optical properties[26–28] of the underlying tissue to obtain the dynamic parameters from the speckle contrast measurements, which limited DSCA to be a qualitative method.

In our previous work,[29] we have developed an approximation model of speckle contrast for flow measurement of turbid media. For simplification, we did not consider the influence of the absorption and assumed that the absorption coefficient is zero. In fact, in addition to the motion of the scattering particles, the presence of optical absorption also can influence the rate of temporal speckle fluctuations and this assumption can result in deviations in the calculated dynamic parameters.[26] As we discuss in this paper, to accurately obtain dynamic parameters from the measured speckle contrast at multiple exposure times, we have developed a more thorough speckle contrast

*Address all correspondence to: Zhonghua Shen, E-mail: shenzh@njust.edu .cn

model to overcome this restriction. We further simplify it to a linear approximation model which describes the linear relation between $1/K^2$ and exposure time, and the dynamic parameter can be obtained from the slope (k_{slope}) of this linear approximation. In fact, k_{slope} is essentially equal to the inverse of the correlation time of the speckle. Then, to validate the theoretical model, we have performed experiments in the liquid phantoms.

This paper is structured as follows: in Sec. 2, we describe the theoretical background of DSCA and deduce the theoretical dependence of speckle contrast on the exposure time based on the correlation diffusion equation (CDE). In addition, the accuracy of the linear approximation model is tested in Sec. 2. In Sec. 3, the experiments are conducted to demonstrate the ability of the slope of this linear model to measure the Brownian diffusion coefficient D_B at different SD separations, by a direct comparison of Einstein diffusion coefficient $D_{B\text{-Einstein}}$ for the liquid phantoms. We show the experimental results in Sec. 4. In Sec. 5, we discuss the influence of the SD separation, optical property, and exposure time on the speckle contrast model for DSCA. Furthermore, the accuracy of the commonly used forms of speckle contrast model is discussed in Sec. 5. Finally, the conclusion about these results is shown in Sec. 6.

2 Theory

2.1 Diffuse Speckle Contrast Analysis

The transport of electric field autocorrelation function $G_1(r, \tau) = \langle E(r, t)E^*(r, t + \tau)\rangle$ in multiple scattering media is governed by the CDE[23,30]

$$\left[-\frac{1}{3\mu_s'}\nabla^2 + \mu_a + \frac{1}{3}\alpha\mu_s'k_0^2\langle\Delta r^2(\tau)\rangle\right]G_1(r, \tau) = S(r), \quad (1)$$

where μ_s' is the reduced scattering coefficient, μ_a is the absorption coefficient, k_0 is the magnitude of the light wave vector in the medium, $\alpha(0-1)$ accounts for the presence of static scatterers and is the fraction of moving scatterers to the total number of scatterers in the medium, $S(r)$ is the light-source distribution, and $\langle\Delta r^2(\tau)\rangle$ is the mean square displacement (MSD) of the moving scatterers (i.e., red blood cells) in time τ. Usually, MSD has been modeled as either unordered (Brownian) motion with $\langle\Delta r^2(\tau)\rangle = 6D_B\tau$, where D_B is the particle diffusion coefficient, or ordered flow with $\langle\Delta r^2(\tau)\rangle = v^2\tau^2$, where v is the root-mean-square speed of the scatterers. Most studies show that the Brownian motion model results in a better fit to the experimental measurements than the random flow model. In addition, other models[31–33] have been used to consider the different types of motion.

The solutions $G_1(r, \tau)$ can be obtained analytically in standard geometries.[22,23,30] For the semi-infinite geometry, the Green's function $G_1(r, \tau)$ of Brownian motion at a distance r from the source is given by

$$G_1(r, \tau) = \frac{3\mu_s'}{4\pi}\left\{\frac{\exp[-K(\tau)r_1]}{r_1} - \frac{\exp[-K(\tau)r_2]}{r_2}\right\}, \quad (2)$$

where $K(\tau) = [3\mu_s'\mu_a + 6\mu_s'^2k_0^2\alpha D_B\tau]^{1/2}$, $r_1 = [r^2 + l_{tr}^2]^{1/2}$, $r_2 = [r^2 + (l_{tr} + 2z_b)^2]^{1/2}$, $l_{tr} = 1/\mu_s'$, r is the SD separation, $z_b = 2(1 - R_{\text{eff}})/3\mu_s'(1 + R_{\text{eff}})$, and R_{eff} is the effective reflection coefficient accounting for the index mismatch between the

tissue and surrounding medium.[34] The normalized electric field correlation function $g_1(r, \tau)$ is shown as

$$g_1(r, \tau) = G_1(r, \tau)/G_1(r, 0). \quad (3)$$

Traditionally, for DCS the motion of scattering particles can be obtained in this geometry from the measured intensity autocorrelation function $g_2(r, \tau)$ of one single speckle by the Siegert relation $g_2(r, \tau) = 1 + \beta|g_1(r, \tau)|^2$, where β is a constant determined by experimental setup.[35] Meanwhile, the motion of scattering particles will also result in the reduction of the detected laser speckle contrast for a given exposure time. The following equation [24] shows the relationship between speckle contrast and the autocorrelation function $g_1(r, \tau)$ in terms of the exposure time T

$$K^2(T) = \frac{2\beta}{T}\int_0^T(1 - \tau/T)[g_1(r, \tau)]^2\mathrm{d}\tau. \quad (4)$$

Usually, the form of speckle contrast depends on the form of $g_1(r, \tau)$ which is based on the number of scattering events and the type of particle motion. Table 1 shows three analytical forms of speckle contrast for three forms of $g_1(r, \tau)$ that are commonly used in LSCI literatures. Here, $x = T/\tau_c$ and τ_c is defined as the correlation time at which the autocorrelation function is equal to the value of $1/e$. For DSCA, we note that the combination of the Green's solution $g_1(r, \tau)$ in Eq. (3) and the expression in Eq. (4) can also be used to obtain dynamic property from the measurements of speckle contrast at different SD separations or exposure times.[36,37] Therefore, it is necessary to derive, a general analytical expression of speckle contrast for the medium with an absorption coefficient μ_a, a reduced scattering coefficient μ_s', and a blood flow index αD_B.

Substituting Eq. (3) into Eq. (4), the speckle contrast expression can be written as

$$K^2(r, T) = \sum_{i=1}^2\sum_{j=1}^2\frac{(-1)^{i+j}}{r_ir_jG_0^2}$$
$$\times\frac{2\beta}{T}\int_0^T(1 - \tau/T)\exp[-(r_i + r_j)$$
$$\times(K_0^2 + F\tau)^{1/2}]\mathrm{d}\tau, \quad (5)$$

where $K_0 = K(\tau = 0) = [3\mu_s'\mu_a]^{1/2}$, $F = 6\mu_s'^2k_0^2\alpha D_B$, and $G_0 = 4\pi G_1(r, 0)/3\mu_s'$. K_0 and G_0 have units of cm^{-1}, and F has units of cm^{-2}/s. Equation (5) is a summation of speckle contrast calculated by the form that is similar to the form $g_1(x) = \exp(-x^{1/2})$ in Table 1. The presence of optical property (K_0) makes this calculation process more complex. The resulting equation, an expression for speckle contrast can be given by

Table 1 Forms of $K^2(x)$ for three forms of commonly used $g_1(x)$.

$g_1(x = \tau/\tau_c)$	$K^2(x = T/\tau_c)$
$\exp(-x)$	$\beta(e^{-2x} - 1 + 2x)/(2x^2)$
$\exp(-\sqrt{x})$	$\beta[(3 + 6\sqrt{x} + 4x)e^{-2\sqrt{x}} - 3 + 2x]/(2x^2)$
$\exp(-x^2)$	$\beta[e^{-2x^2} - 1 + \sqrt{2\pi}x\text{erf}(\sqrt{2}x)]/(2x^2)$

$$K^2(r,T) = \frac{8\beta}{(FT)^2 G_0^2} \sum_{i=1}^{2} \sum_{j=1}^{2} \frac{(-1)^{i+j}}{r_i r_j (r_i + r_j)^4}$$

$$\times [X_{ij}(T) - X_{ij}(0) + Y_{ij} FT],$$

$$X_{ij}(T) = \left[(r_i + r_j)^2 (K_0^2 + FT) + 3(r_i + r_j)\sqrt{K_0^2 + FT} \right.$$

$$\left. + 3 \right] \times e^{-(r_i + r_j)\sqrt{K_0^2 + FT}},$$

$$Y_{ij} = \frac{1}{2}(r_i + r_j)^2 [1 + K_0(r_i + r_j)] \times e^{-K_0(r_i + r_j)}. \quad (6)$$

Equation (6) is a general formula that describes the typical behavior of speckle contrast K with respect to the exposure time T and the SD separation r. For a given tissue, this equation provides us a physical model to obtain the dynamic property αD_B of the diffuse media from the measurements of speckle contrast K by MESI. In the following section, we will use Eq. (6) to calculate the corresponding speckle contrast as a function of exposure time and the SD separation.

2.2 Linear Approximation for Diffuse Speckle Contrast Analysis

The MESI uses the dependence of the speckle contrast on camera exposure time via a mathematical model (Table 1) to obtain blood flow changes by extracting the characteristic correlation time of the speckles. With the analytical expression of Eq. (6), the accurate estimation of particles' Brownian motion can be obtained from speckle contrast measurements at multiple exposure times. However, the speckle contrast model of Eq. (6) in the DSCA is so complicated that this nonlinear fitting may be very time-consuming and even may result in nonconvergence for some speckle contrast measurements in many practical conditions. To make MESI work well in DSCA, we need to develop a simpler mathematical model to provide comparable accurate measurements of particles' Brownian motion compared with Eq. (6). In this section, we discuss the linear approximation, i.e., the linear relation between $1/K^2$ and exposure time T.

The inverse of speckle contrast can be written as

$$\frac{1}{K^2(r,T)} = \frac{(FT)^2}{8\beta[\chi FT - \gamma(T)]},$$

$$\chi = \frac{1}{G_0^2} \sum_{i=1}^{2} \sum_{j=1}^{2} \frac{(-1)^{i+j}}{r_i r_j (r_i + r_j)^4} Y_{ij},$$

$$\gamma(T) = \frac{1}{G_0^2} \sum_{i=1}^{2} \sum_{j=1}^{2} \frac{(-1)^{i+j}}{r_i r_j (r_i + r_j)^4} [X_{ij}(0) - X_{ij}(T)], \quad (7)$$

where χ has units of cm^{-2} and $\gamma(T)$ has units of cm^{-4}.

Rearranging Eq. (7), $1/K^2(r,T)$ can be described by

$$\frac{1}{K^2(r,T)} = \frac{1}{\beta}\left[\frac{F}{8\chi}T + \lambda(T)\right],$$

$$\lambda(T) = \frac{1}{8\chi} \times \frac{\gamma(T)}{\chi - \frac{\gamma(T)}{FT}}, \quad (8)$$

where $\lambda(T)$ is dimensionless. We note that $\lambda(T)$ decreases with the increasing of exposure time T. $\lambda(T)$ has the maximum value

$\lambda(T)_{\max} = 1$ when the exposure time is equal to 0. On the other hand, when the exposure time tends to be infinite, $\lambda(T)$ has the minimum value and can be written as

$$\lambda(T)_{\min} = \frac{1}{8\chi^2 G_0^2} \sum_{i=1}^{2} \sum_{j=1}^{2} \frac{(-1)^{i+j}}{r_i r_j (r_i + r_j)^4} X_{ij}(0). \quad (9)$$

Then $1/K^2(r,T)$ is bounded by two lines with the same slope ($k_{\text{slope}} = F/8\beta\chi$), i.e.,

$$\frac{1}{\beta}\left[\frac{F}{8\chi}T + \lambda(T)_{\min}\right] \leq \frac{1}{K^2(r,T)} \leq \frac{1}{\beta}\left[\frac{F}{8\chi}T + 1\right]. \quad (10)$$

When the exposure time is larger than correlation time, the change of $\lambda(T)$ due to the change of T is relatively smaller than $1/K^2(r,T)$ in Eq. (10). Therefore, $1/K^2(r,T)$ can be approximatively described by a linear equation

$$\frac{1}{K^2(r,T)} = \frac{1}{\beta}\left(\frac{F}{8\chi}T + b_{\text{in}}\right) = \frac{1}{\beta}\left(\frac{3\mu_s'^2 k_0^2 \alpha D_B}{4\chi}T + b_{\text{in}}\right), \quad (11)$$

where b_{in} is the intercept and is within the range determined by Eq. (10). b_{in} can be obtained from the linear fitting of the measurements $1/K^2$ at different exposure times. We note that the slope k_{slope} of this linear equation provides the ability to extract the flow information αD_B. Compared with Eq. (6), this linear equation [Eq. (11)] has the advantage of simplicity. We next quantify the range of exposure time for which this linear approximation can be accurately employed.

The theoretical $1/K^2$ values were calculated from the analytical solution of Eq. (6) at the SD separation $r = 1$ cm as shown in Fig. 1(a). Here we have used $\mu_a = 0.1$ cm^{-1}, $\mu_s' = 10$ cm^{-1}, $\alpha D_B = 2 \times 10^{-8}$ cm^2/s, the medium refractive index $n = 1.33$, $\beta = 1$, and $\lambda = 671$ nm for the calculation. Figure 1(a) shows the relation between $1/K^2$ and T (ms in units) can be described by the linear fitting $1/K^2 = 28.65T + 0.77$ ($R^2 = 1$) for a wide range of exposure times. We calculated the theoretical value of k_{slope} and the range of b_{in} by Eqs. (11) and (9), i.e., $k_{\text{slope}} = 28.70$ ms^{-1} and $0.613 \leq b_{\text{in}} \leq 1$. We note that good agreement between the linear fitting in Fig. 1(a) and the theoretical value is found, and the difference of k_{slope} is relatively small. In addition, for more effectively observing this linear fitting at small exposure times, Fig. 1(b) shows the comparison results of speckle contrast calculated by Eq. (6) and this linear fitting (red line), respectively. The green lines in Fig. 1(b) represent theoretical K^2 from the linear equation with $b_{\text{in}} = 0.613$ and $b_{\text{in}} = 1$, respectively. Note that a log time scale in Fig. 1(b) has the same exposure time as a linear time scale in Fig. 1(a), and is used to better observe the shape of each curve. As shown in Fig. 1(b), when the exposure time is smaller than the correlation time [$\tau_c = 0.035$ ms obtained from $g_1(r,\tau)$], this linear fitting has some obvious discrepancies. The shorter exposure time makes b_{in} tend to be 1 and the change in b_{in} results in a larger fluctuation in K^2 when $T < \tau_c$.

We note that $k_{\text{slope}} = 28.65$ ms^{-1} and $b_{\text{in}} = 0.77$ in Fig. 1(a) were obtained by fitting the theoretical $1/K^2$ values at multiple exposure times. In addition, the numerical slope values $k_{\text{slope}}(T)$ at different exposure times can be obtained by the relation $k_{\text{slope}}(T) = (1/K^2 - b_{\text{in}})/T$ in which the calculated $1/K^2$ and
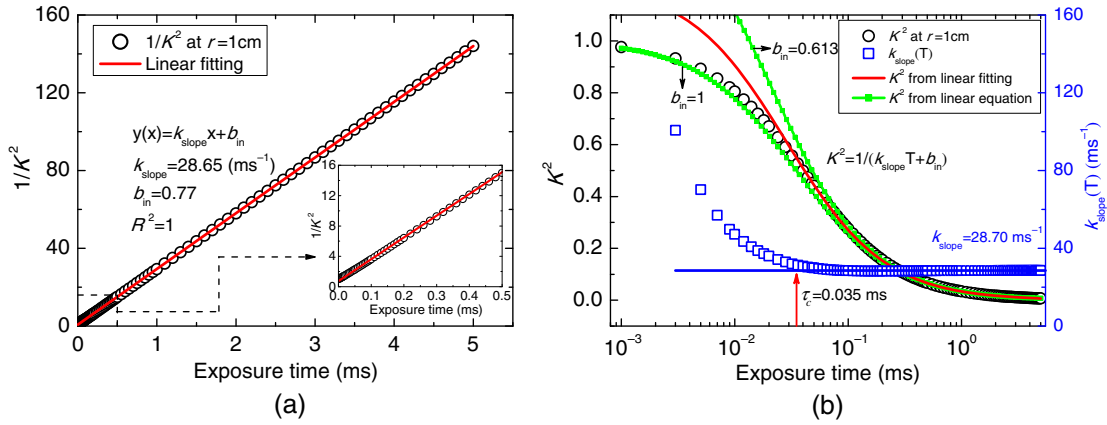
Fig. 1 Linear approximation for DSCA. (a) The calculated $1/K^2$ and (b) K^2 from Eq. (6) as a function of exposure time at $r = 1$ cm. The red line $1/K^2 = 28.65 T + 0.77$ is the result of the linear fitting. The blue square in (b) corresponds to the numerical values $k_{\text{slope}}(T)$. The green lines in (b) represent theoretical K^2 from the linear equation with $k_{\text{slope}} = 28.70$ ms^{-1}, $b_{\text{in}} = 0.613$ and $b_{\text{in}} = 1$, respectively. $\tau_c = 0.035$ ms. Here $n = 1.33$, $\beta = 1$, $\lambda = 671$ nm, $\mu_a = 0.1$ cm^{-1}, $\mu_s' = 10$ cm^{-1}, and $\alpha D_B = 2 \times 10^{-8}$ cm^2/s.

$b_{\text{in}} = 0.77$ in Fig. 1(a) were used. Figure 1(b) plots the comparison results between these numerical values $k_{\text{slope}}(T)$ (blue square) and $k_{\text{slope}} = 28.70$ ms^{-1} (blue line) and shows that the choice of the linear approximation model is accurate when $T > \tau_c$. In addition, we note that the theoretical $k_{\text{slope}} = 28.70$ ms^{-1} is nearly equal to the inverse of the correlation time $1/\tau_c = 28.60$ ms^{-1}. Theoretical demonstration of this equivalence is described and given in Appendix A. Thus, the use of this linear approximation can provide comparable accurate measurements of flow information αD_B from k_{slope}.

3 Experimental Method

3.1 Tissue Simulating Phantoms

To demonstrate that we can use k_{slope} to extract the dynamic property of a diffusive medium, we have designed a phantom experiment as shown in Fig. 2. Liquid phantom comprises Intralipid (30%, Fresenius Kabi, China), India ink (Black 4001, Pelikan, Germany), and distilled water. The theory and details of Intralipid including optical properties and particle radius were described in Ref. 38. The Intralipid particles in liquid phantom provided Brownian motion and the reduced scattering coefficient μ_s' of the phantom. India ink behaved as the absorber and controlled the absorption coefficient μ_a of the phantom. The optical properties of India ink show larger brand-to-brand and batch-to-batch variations.[39] However, the
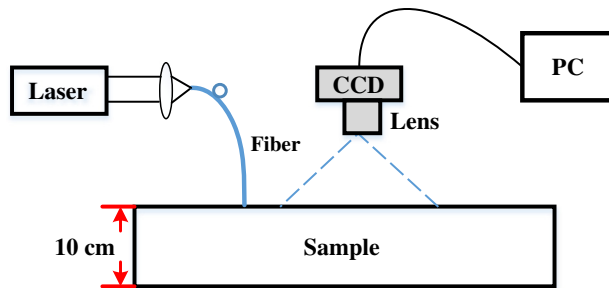
ratio (μ_a/μ_e) between the absorption and the extinction coefficient μ_e of India ink remains constant.[39] Therefore, we have measured the extinction coefficient of India ink used in this paper at $\lambda = 671$ nm by an experimental setup described in Ref. 40. The extinction coefficient μ_e was obtained from the collimated transmittance as a function of the ink concentration, i.e., $\mu_e = 524.6$ mm^{-1}. Using the constant ratio $\mu_a/\mu_e = 0.839$ in Ref. 39, we obtained the absorption coefficient $\mu_a = 440.1$ mm^{-1}. The absorption coefficient of distilled water is taken from Ref. 41. The 30% Intralipid and India ink were diluted by distilled water to obtain the desired optical properties of the phantom with $\mu_s' = 10$ cm^{-1} and $\mu_a = 0.1$ cm^{-1}.

A continuous laser source at 671 nm (CNI MRL-III-671, 100 mW) was coupled to a 200 μm multimodel optical fiber and illuminated the surface of the phantom. The backscattering speckle patterns were recorded by a 12-bit CCD camera (IMC-140F, Imi Tech, Korea). A lens with $f = 50$ mm and $f/\# = 8$ was used to provide the field of view 1.4 cm $\times$ 1.2 cm, resulting in a pixel diameter of 1.0×10^{-3} cm. The transparent container filled by the liquid had the square cross section of 10 cm size.

3.2 Brownian Motion of the Particles in Phantoms

To verify the experimental results, we estimated the value of the Brownian diffusion coefficient based on the Stokes–Einstein formula as a comparison. The Intralipid particles in phantoms provided Brownian motion and all Intralipid scatterers in the phantom were considered dynamic with $\alpha = 1$. Then the effective Brownian diffusion coefficient should be equal to the Einstein diffusion coefficient $D_{B\text{-Einstein}}$

$$D_{B\text{-Einstein}} = \frac{k_B T}{6\pi R \eta}, \quad (12)$$

where k_B is the Boltzmann constant, T is the temperature, R is the radius of the particles, and η is the viscosity. The viscosity of the phantom at 18°C was measured by a viscometer with a value of 1.10 ± 0.031 cp (centipoise). The diameters of the particles vary from 25 nm to hundreds of nm for the Intralipid and the average radius of Intralipid particles was estimated as 87.1 nm

Fig. 2 Schematic diagram of the experimental setup using the phantom.

from Ref. 38. Then the Brownian diffusion coefficient can be calculated by the measured viscosity and the particle radius, i.e., $D_{B\text{-Einstein}} = 2.22 \times 10^{-8} \text{ cm}^2/\text{s}$.

3.3 Data Analysis

We further present an experiment where the Brownian diffusion coefficients at different SD separations were obtained from the speckle contrast measurements at different exposure times. We have defined seven detector regions with a size of 15×15 pixels ($0.15 \times 0.15 \text{ mm}^2$) at different SD separations ranging from 0.6 to 1.8 cm. For each SD separation, the exposure time ranging from 0.1 to 1 ms with a step size of 0.1 ms was used and 40 images were obtained for each exposure time. For each image of each detector, we used a 7×7 window size to calculate the speckle contrast and further obtained a spatially averaged speckle contrast over the detector region. Then these speckle contrasts were temporally averaged over 40 images. Meanwhile, for reducing the influence of the dark and shot noise[36,37,42] on the calculation of speckle contrast, we used the method described in Ref. 36 to correct the influence of the noise.

The Brownian diffusion coefficient D_B was obtained by two different ways. One was that a non-linear least squares fit written by MATLAB (Lsqcurvefit with Levenberg–Marquardt algorithm, Mathwork, Inc.) was performed to obtain D_B by minimizing the difference between the measured speckle contrasts versus multiple exposure times and the analytical solution of Eq. (6) with known optical property. The other way was the linear fitting and D_B was obtained from the slope of the linear fitting. We note that β depending on experimental condition was *a priori* estimated from the static speckle contrast, which made the nonlinear fitting process computationally less intensive and the linear fitting to have the ability to obtain D_B from k_{slope}.

4 Results

4.1 Validation with Theoretical Data

We tested linear approximation model using the theoretical data (Fig. 3), as well as experimental data from the liquid phantom (Figs. 4 and 5). The theoretical speckle contrast data were calculated from analytical solution of Eq. (6) with $\beta = 0.124$. The

parameters for the calculated data, such as optical properties, β, Brownian diffusion coefficient D_B, exposure time, and SD separation etc., were the same as the experiment. Figure 3(a) shows the theoretical $1/K^2$ for seven SD separations plotted as a function of exposure time. The linear fitting was then applied to the theoretical speckle contrast at exposure times ranging from 0.1 to 1 ms with a step size of 0.1 ms and the goodness of fit was very high (the averaged R^2 over seven fits = 0.9999). The obtained parameter $D_{B\text{-linear}}$ from k_{slope} is compared with the theoretical D_B as shown in Fig. 3(b). Good agreement between the calculated and actual D_B is found for seven SD separations and the relative error is no more than 0.57%. In addition, the intercept b_{in} of the linear fitting at different SD separations is also shown in Fig. 3(b). The black dashed lines represent the upper and lower bound of the intercept, which were calculated from Eq. (10). We note that the intercept b_{in} decreases with the increasing of SD separation, which is a consequence of the fact that when SD separation increases, the autocorrelation function decays more quickly and the correlation time decreases. In summary, these theoretical results provide the evidence in favor of our linear approximation model.

4.2 Validation with Experimental Data

The speckle contrasts at different SD separations are plotted against the exposure time as shown in Fig. 4(a). It can be observed that for all exposure times, we have usable speckle contrast measurements up to 1.0 cm. When the exposure time is increased to 0.3 ms, the SD separation is extended to 1.8 cm. Meanwhile, the speckle contrast curves of larger SD separation decay more quickly with exposure time. The speckle contrast measurements of each SD separation were then fitted to Eq. (6) using the nonlinear least square method and the estimated value of $\beta = 0.124$. Figure 4(a) clearly shows that the speckle contrast model of Eq. (6) fits the experimental data very well and the calculated Brownian diffusion coefficient D_B is shown in Fig. 4(b). The Brownian diffusion coefficient D_B is not expected to change along the SD separation. Indeed, the Brownian diffusion coefficient D_B shows good stability with a mean D_B of $2.14 \times 10^{-8} \text{ cm}^2/\text{s}$ and standard deviation between SD separation of $0.079 \times 10^{-8} \text{ cm}^2/\text{s}$,
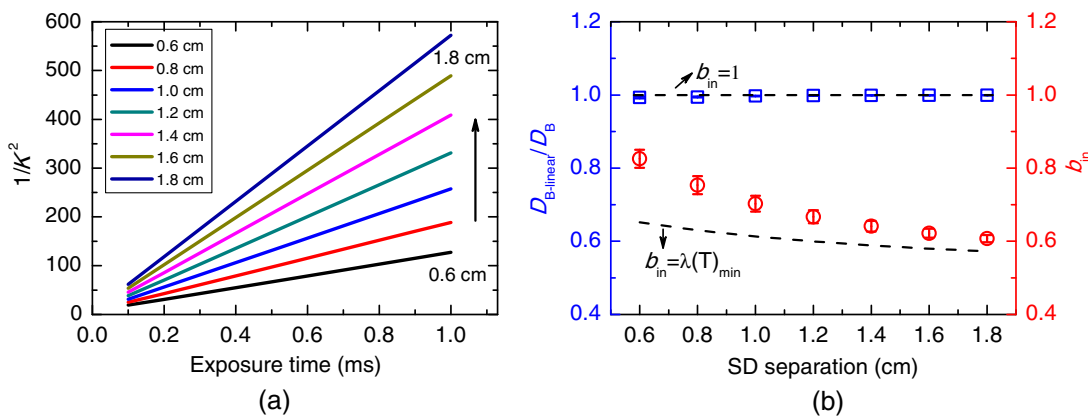
Fig. 3 (a) Theoretical $1/K^2$ at seven SD separations as a function of exposure time. The parameters used for the calculation are $\beta = 0.124$, $n = 1.33$, $\lambda = 671$ nm, $\mu_a = 0.1 \text{ cm}^{-1}$, $\mu_s' = 10 \text{ cm}^{-1}$, and $D_B = 2.22 \times 10^{-8} \text{ cm}^2/\text{s}$. (b) The calculated $D_{B\text{-linear}}/D_B$ and the intercept b_{in} from the linear fitting for different SD separations. The black dashed lines in (b) are the range calculated by Eq. (10) and the estimated b_{in} is bounded by two dashed lines. Error bars are the standard deviations.

(a)

(b)
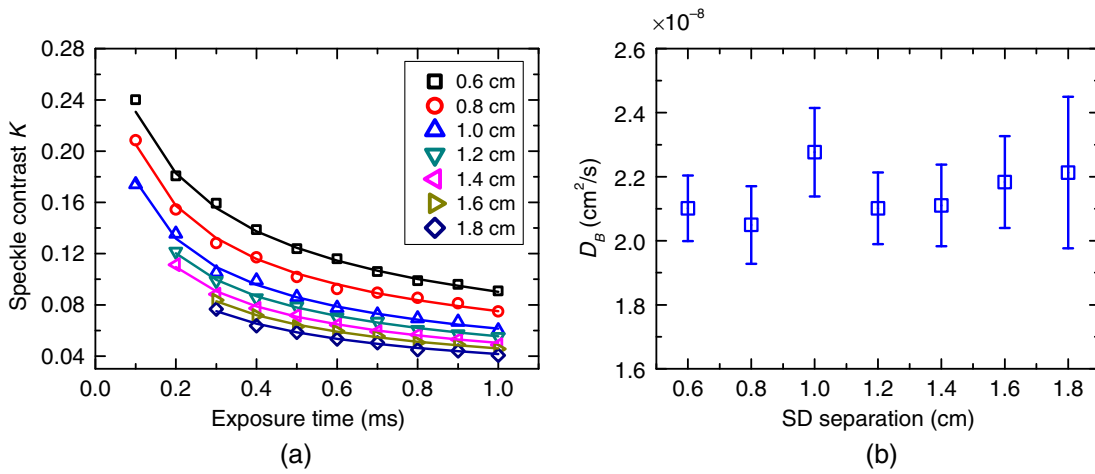
Fig. 4 Performance of speckle contrast model of Eq. ([6](#)) in DSCA. (a) The speckle contrast measurements versus exposure time at different SD separations are fitted to obtain the results of (b) the Brownian diffusion coefficient D_B.

which is in agreement with the measured value $D_{B\text{-Einstein}} = 2.22 \times 10^{-8}$ cm^2/s.

After showing that the speckle contrast model of Eq. ([6](#)) is able to measure D_B, we present the performance of the linear approximation model in DSCA as shown in Fig. [5](#). Figure [5(a)](#)

shows that the $1/K^2$ measurements follow a linear relationship with exposure time and the average R^2 over seven fits is 0.995. Then the Brownian diffusion coefficient $D_{B\text{-linear}}$ and b_{in} were calculated from the linear fitting by the estimated value of β and Eq. ([11](#)). The Brownian diffusion coefficient $D_{B\text{-linear}}$ in

(a)

(b)

(c)

(d)
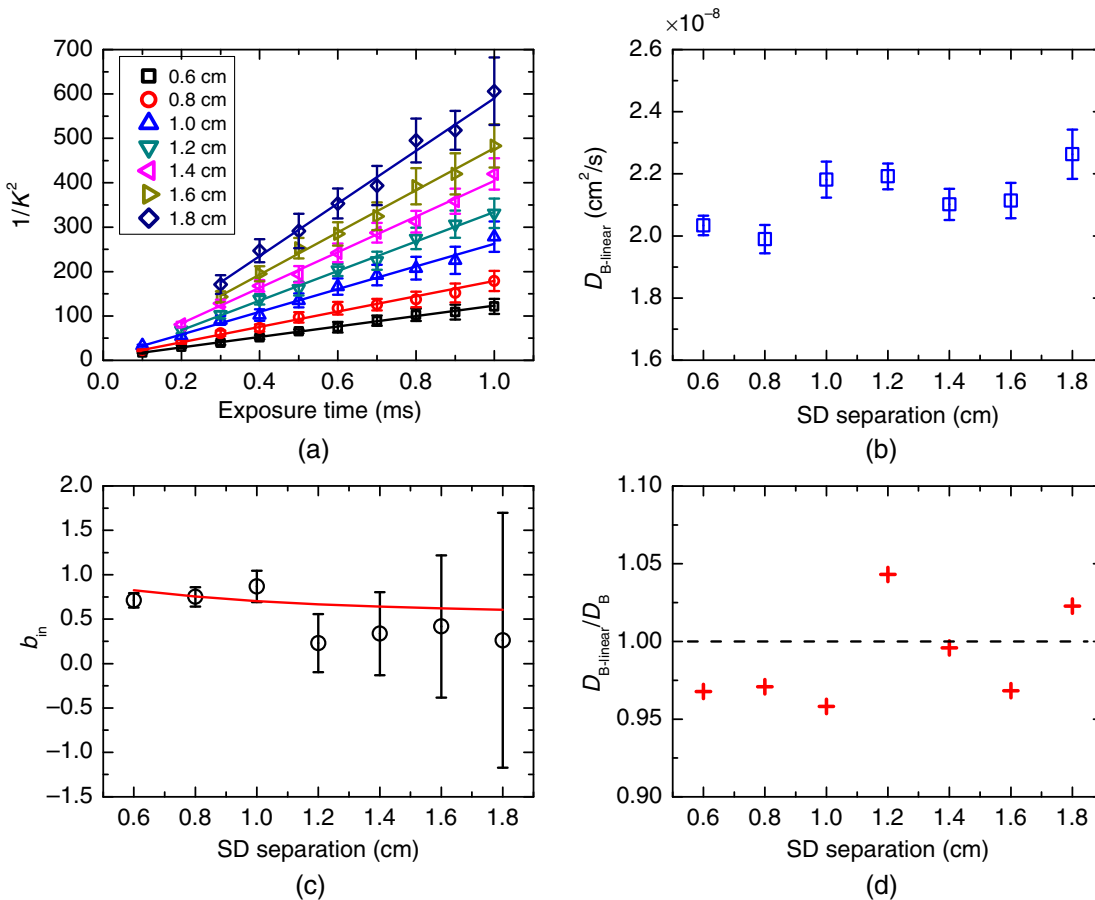
Fig. 5 Performance of linear approximation model in DSCA (a) The measurements of $1/K^2$ at multiexposure time (data points) and corresponding linear fitting (lines) for different SD separations. Fit parameter (b) $D_{B\text{-linear}}$ and (c) b_{in} from the calculated k_{slope} and the intercept of the linear fitting, respectively. The red line in (c) is obtained from the result of Fig. [3(b)](#). (d) The comparison between $D_{B\text{-linear}}$ and D_B from Fig. [4(b)](#). β was estimated at 0.124.

Fig. 5(b) also shows good stability along SD separation and has a mean of 2.12×10^{-8} cm^2/s. The standard deviation of $D_{B\text{-linear}}$ between SD separations is 0.095×10^{-8} cm^2/s and the mean standard deviation of $D_{B\text{-linear}}$ is 0.052×10^{-8} cm^2/s. Figure 5(c) shows the comparison result of b_{in} with the theoretical results in Fig. 3(b) [red line in Fig. 5(c)]. Both results are again in agreement with the theoretical value. We note that the percentage errors in estimates of b_{in} increase with the increasing of SD separation, which is due to the speckle contrast sensitivity[43,44] for exposure time at different SD separations. In addition, we have quantified the difference between $D_{B\text{-linear}}$ and D_B obtained by the speckle contrast model of Eq. (6) in Fig. 4(b). Figure 5(d) shows that this difference is relatively small and the relative error is no more than 5% for different SD separations. Thus, this linear approximation model can provide comparable accurate measurement of the Brownian diffusion coefficient compared with the speckle contrast model of Eq. (6).

5 Discussion

The DSCA has been employed extensively in the biomedical optics[24,25,45–47] because of its simplicity. In order to make the recovery of flow information from speckle contrast measurements, it is necessary to obtain the speckle contrast analytical models that have been already well established in the LSCI. In this work, we first deduced the theoretical behavior of speckle contrast with respect to exposure time and SD separation as shown in Eq. (6). The speckle contrast measurements were then fitted to Eq. (6) to obtain a quantitative recovery of effective dynamic parameter D_B as shown in Fig. 4. Meanwhile, we have demonstrated the accuracy of the linear relation between $1/K^2$ and exposure time in both theory (Figs. 1 and 3) and experimental data (Fig. 5). The theoretical behavior of $1/K^2$ with respect to the exposure time can be essentially separated in two parts, one with a fixed slope $k_{slope}T$ and the other $\lambda(T)$ as shown in Eq. (8). $\lambda(T)$ depends on the exposure time and decreases with the increasing of the exposure time. Therefore, the theoretical $1/K^2$ is bounded by two lines with the same slope k_{slope}. When the exposure time is larger than correlation time, the change in $\lambda(T)$ is relatively smaller than $1/K^2$ and then $1/K^2$ can be approximatively described by a linear equation of Eq. (11) within the range of two lines. To validate the theoretical model, we have performed experiments in tissue liquid phantoms. Our results show that it is possible to accurately obtain the Brownian diffusion coefficient $D_{B\text{-linear}}$ at different SD separations from the slope k_{slope} of this linear relation by a direct comparison to the theoretical model of Eq. (6). Furthermore, we have demonstrated that k_{slope} is equal to the inverse of correlation time ($1/\tau_c$) of the speckle as shown in Appendix A. This agreement indicates that the Brownian diffusion coefficient also can be rapidly recovered from the correlation time of the measured $g_2(r, \tau)$ curve by DCS. Meanwhile, for actual applications, some important effects on the DSCA need further to be discussed.

5.1 Dependence of Speckle Contrast on Source–Detector Separation

We have used the dependence of speckle contrast on the exposure time at a certain SD separation to obtain D_B as mentioned above. In fact, the measurement of D_B also can be performed by the speckle contrast measurements at multiple SD separations for a fixed exposure time as shown in Fig. 6. The nonlinear least square method is used in Fig. 6(a) to describe the dependence of speckle contrast on SD separation by Eq. (6). It can be observed that we use the exposure time in Fig. 6(b) at which we have speckle contrast measurements up to 1.8 cm. The fitted D_B in Fig. 6(b) has a mean of 2.13×10^{-8} cm^2/s, which is again in agreement with the value of $D_{B\text{-Einstein}} = 2.22 \times 10^{-8}$ cm^2/s. Thus, the different fitting ways of Eq. (6), i.e., the dependence of speckle contrast on multiple exposure time, or SD separations, are both valid to obtain D_B for DSCA.

5.2 Influence of Optical Property on D_B Measurements

DSCA is not inherently able to measure D_B without *a priori* knowledge of the optical properties of the diffusive medium. We have demonstrated that D_B can be calculated from the calculated k_{slope} of the linear approximation model using the known μ_s' and μ_a. However, the inaccurate estimation of μ_s' and μ_a will result in the error in the calculated D_B. Therefore, we need to theoretically quantify the flow index D_B errors due to the inaccurate estimation of μ_s' and μ_a. The percentage error is defined as [(inaccurate − true)/true] × 100%. $D_{B\text{-True}}$ calculated from k_{slope}
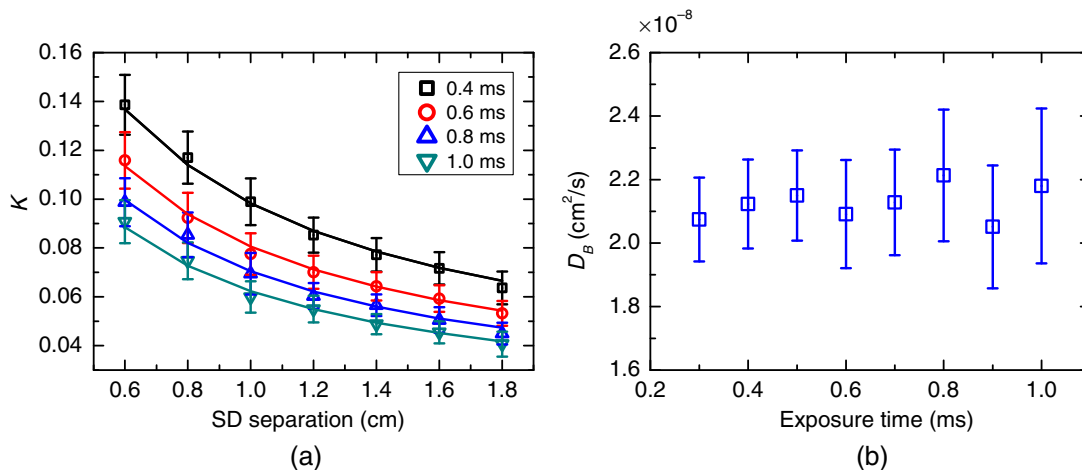
Fig. 6 (a) Speckle contrast measurements versus SD separation at different exposure time and the corresponding nonlinear fittings by Eq. (6). (b) The fitted parameter D_B at different exposure time.

using the true value of $\mu'_{s\text{-True}}$ and $\mu_{a\text{-True}}$ is considered as true value. $D_{B\text{-Inac}}$ is considered as an inaccurate value which is calculated from the inaccurate value of $\mu'_{s\text{-Inac}}$ and $\mu_{a\text{-Inac}}$. Then the percentage errors for μ'_s and μ_a are $[(\mu'_{s\text{-Inac}} - \mu'_{s\text{-True}})/\mu'_{s\text{-True}}] \times 100\%$ and $[(\mu_{a\text{-Inac}} - \mu_{a\text{-True}})/\mu_{a\text{-True}}] \times 100\%$, respectively. The percentage error of D_B is written as

$$\text{Error in } D_B = \left[\frac{\mu'_{s\text{-True}}}{\mu'_{s\text{-Inac}}} \times \frac{\chi(\mu'_{s\text{-Inac}}, \mu_{a\text{-Inac}})}{\chi(\mu'_{s\text{-True}}, \mu_{a\text{-True}})} - 1 \right] \times 100\%.$$

(13)

Equation (13) shows that the laser wavelength and the medium refractive index do not play a role in determining the error of the calculated D_B due to the variation of optical property. We note that the authors[26] have used liquid phantoms with controlled variations of optical properties to isolate the influence of μ'_s and μ_a on the accuracy of D_B by the analysis of $g_2(r, \tau)$ curve in DCS. In fact, the influence of μ'_s and μ_a on the accuracy of D_B depends on the correlation time τ_c of $g_2(r, \tau)$ curve. Theoretically, DSCA is obtained from $g_2(r, \tau)$ by temporal integration and we have demonstrated that k_{slope} is equal to $1/\tau_c$ in Appendix A. Therefore, the theoretical result of Eq. (13) can be used to demonstrate the experimental results in Ref. 26. Figure 7 shows the influence of the percentage errors for μ'_s and μ_a on the percentage D_B error. The parameters used for the calculation of Eq. (13), including $\mu'_{s\text{-True}}$ from 0.05 to 0.2 cm^{-1}, $\mu_{a\text{-True}}$ from 4 to 16 cm^{-1}, SD separation 2.8 cm, $\mu'_{s\text{-Inac}} = 10$ cm^{-1}, and $\mu_{a\text{-Inac}} = 0.125$ cm^{-1}, are the same as Ref. 26. As shown in Fig. 7, μ'_s has a much greater influence on the estimates of D_B than μ_a. Underestimated μ'_s or $\mu_a - 37.5\%$ results in D_B error of $+112\%$ or -17%, and overestimated μ'_s or $\mu_a + 150\%$ leads to -77% or $+39\%$ regardless of the wavelengths used, which are in good agreement with the experimental results in Ref. 26. These theoretical results further provide the evidence in favor of the works in Ref. 26. In addition, we note that the error in D_B due to other ranges of optical property at different SD separations can also be obtained from Eq. (13).

5.3 Influence of Exposure Time on Diffuse Speckle Contrast Analysis

Similar to LSCI, the exposure time also plays an important role in DSCA. In this paper, the range of exposure time 0.1 to 1 ms
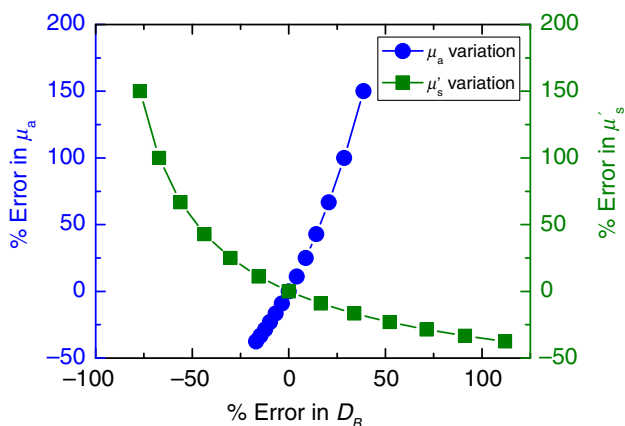
was used to obtain the Brownian diffusion coefficient, considering the sensitivity of speckle contrast and SNR. Unlike LCSI, the use of multiple exposures does not capture the full shape of $1/K^2$ with exposure time T for DSCA, especially for the exposure time in which the speckles have not decorrelated. Therefore, it is difficult to separate the value of β and D_B by performing the nonlinear fitting of the multiple-exposure measurements to the speckle contrast model of Eq. (6). Here a priori estimated β was used in this paper to reduce the computational complexity of the fitting process. In fact, the exposure time can be further reduced but this results in reducing SNR. These effects need to be further discussed in the future. In addition, the number of the exposure times needed for the convergence of the linear model and the computational simplicity make this linear model a relatively fast method.

5.4 Accuracy of Commonly Used Speckle Contrast Models

As a comparison, we also show the accuracy of the most commonly used speckle contrast expressions in Table 1. As shown in Fig. 8, the speckle contrast model calculated by exponential form $g_1(x) = \exp(-x)$ provides a good match to the shape of speckle contrast decay in the DSCA. The speckle contrast K^2 in Fig. 8 is the same as Fig. 1(b). The differences among the three models are more prominent at the lower exposure time. The decay provided by the speckle contrast function calculated by $g_1(x) = \exp(-x^{1/2})$ appears too fast, while the decay predicted by $g_1(x) = \exp(-x^2)$ shows too slow. We note that the difference among the three models is mostly related to the form of $g_1(r, \tau)$ at the small delay-time. Meanwhile, we can simplify the correlation function $g_1(r, \tau)$ to exponential at the small delay-time (see Appendix B), i.e.,

$$g_1(r, \tau) = \exp\left[-\frac{Fr_1^2 \tau}{2(r_1 K_0 + 1)} \right].$$

(14)

Therefore, the speckle contrast model calculated by exponential form has the smallest error for the three models and the relative error of the fitted parameter τ_c for this model is 9.72%. However, compared with the speckle contrast model

Fig. 7 Percentage D_B error due to the inaccurate estimations of μ'_s and μ_a at the SD separation $r = 2.8$ cm.
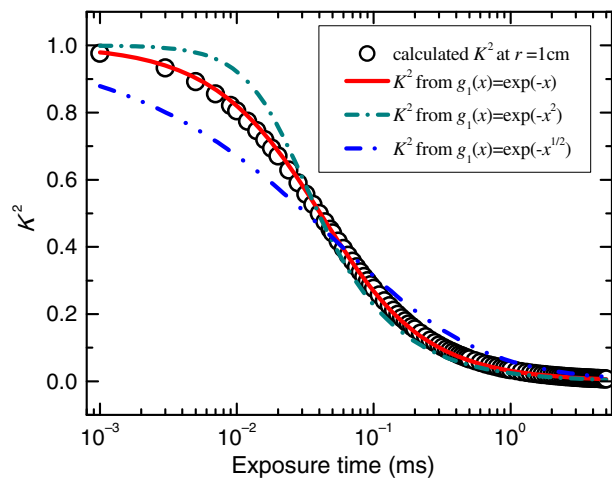
Fig. 8 Calculated K^2 versus exposure time compared with three forms of speckle contrast function calculated by three different forms of $g_1(x)$. The parameters used for the calculation are the same as in Fig. 1.
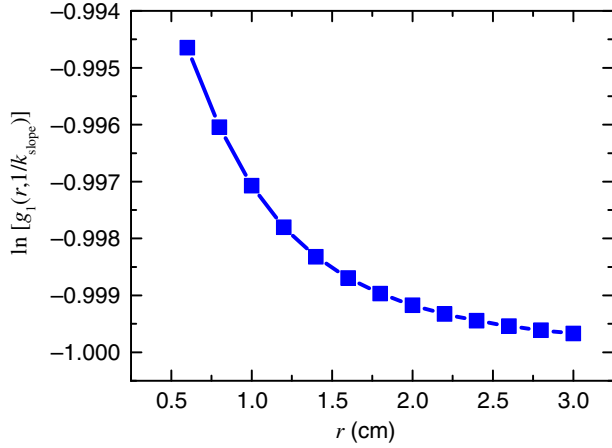
Fig. 9 Calculated $\ln[g_1(r, 1/k_{\text{slope}})]$ plotted as a function of SD separation r. $g_1(r, 1/k_{\text{slope}})$ is obtained by substituting the expression of k_{slope} to the autocorrelation function of Eq. (3). The difference between k_{slope} and $1/\tau_c$ decreases with the increasing of SD separation. However, the difference is small enough and k_{slope} is approximately equal to $1/\tau_c$. Here $n = 1.33$, $\beta = 1$, $\lambda = 671$ nm, $\mu_a = 0.1$ cm^{-1}, and $\mu'_s = 10$ cm^{-1}.

of Eq. (6), this model calculated by exponential form is not able to accurately extract D_B.

6 Conclusions

In summary, we have deduced and experimentally demonstrated the ability of the speckle contrast model of Eq. (6) in DSCA to quantitatively obtain dynamic parameters D_B of diffuse medium, using the dependence of speckle contrast on exposure time and the SD separation. Furthermore, this speckle contrast model can be simplified to be a linear approximation model and the slope k_{slope} of this linear relation is equal to the inverse of correlation time of the speckles. Therefore, the Brownian diffusion coefficient D_B of the turbid media can be rapidly obtained from the slope of this linear relation. The measurement of D_B from this linear model is more accurate compared with speckle contrast model of Eq. (6). Meanwhile, utilizing the k_{slope} expression, we also theoretically quantify the measured D_B errors due to the inaccurate estimation of the optical properties. These results facilitate the quantitative flow measurement in DSCA.

Appendix A

To demonstrate k_{slope} is equal to the inverse of correlation time $1/\tau_c$, first note that the Green's function $g_1(r, \tau)$ is derived from

the radiative transfer equation using diffusion approximation. Usually diffuse approximation is valid when the source–detector separation r is much greater than the transport mean-free path, i.e., $r \gg l_{tr}$. So r_2 can be approximately given by

$$r_2 = [r_1^2 + 2z^2]^{1/2} \approx r_1 + \frac{z^2}{r_1}, \quad \frac{1}{r_2} \approx \frac{1}{r_1}\left(1 - \frac{z^2}{r_1^2}\right), \quad (15)$$

where $z = [2z_b(z_b + l_{tr})]^{1/2}$. The Green's function $G_1(r, \tau)$ of Brownian motion is shown as

$$G_1(r, \tau) = \frac{3\mu'_s}{4\pi r_1}\left\{\exp[-K(\tau)r_1] - \frac{r_1}{r_2}\exp[-K(\tau)r_2]\right\}, \quad (16)$$

where $K(\tau) = \sqrt{K_0^2 + F\tau}$. Since the difference between r_1 and r_2 is relatively small, $K(\tau = 1/k_{\text{slope}})$ can be written as

$$K\left(\tau = \frac{1}{k_{\text{slope}}}\right) = \sqrt{K_0^2 + 8\chi}$$

$$= \sqrt{K_0^2 + \frac{4}{G_0^2}\sum_{i=1}^{2}\sum_{j=1}^{2}\frac{(-1)^{i+j}}{r_i r_j}e^{-K_0(r_i+r_j)}\frac{1 + K_0(r_i+r_j)}{(r_i+r_j)^2}}$$

$$\approx \sqrt{K_0^2 + \frac{4[1 + K_0(r_1+r_2)]}{G_0^2(r_1+r_2)^2}\sum_{i=1}^{2}\sum_{j=1}^{2}\frac{(-1)^{i+j}}{r_i r_j}e^{-K_0(r_i+r_j)}}. \quad (17)$$

We note that G_0 is defined as

$$G_0^2 = \left[\frac{4\pi}{3\mu'_s}G_1(r, 0)\right]^2 = \sum_{i=1}^{2}\sum_{j=1}^{2}\frac{(-1)^{i+j}}{r_i r_j}e^{-K_0(r_i+r_j)}, \quad (18)$$

which results in the expression for $K(\tau = 1/k_{\text{slope}})$ reducing to

$$K\left(\tau = \frac{1}{k_{\text{slope}}}\right) = K_0 + \frac{2}{r_1 + r_2}. \quad (19)$$

Therefore, the autocorrelation function $g_1(r, \tau)$ at $\tau = 1/k_{\text{slope}}$ can be approximately given by

$$g_1\left(r, \frac{1}{k_{\text{slope}}}\right) = \frac{\exp(-K_0 r_1)\exp\left(-\frac{r_1 - r_2}{r_1 + r_2}\right) - \frac{r_1}{r_2}\exp(-K_0 r_2)\exp\left(-\frac{r_2 - r_1}{r_1 + r_2}\right)}{\exp(-K_0 r_1) - \frac{r_1}{r_2}\exp(-K_0 r_2)} \times \exp(-1)$$

$$\approx \exp(-1). \quad (20)$$

In addition, we also can obtain $g_1(r, 1/k_{\text{slope}})$ by the means of numerical computation as shown in Fig. 9. Both results have demonstrated that $k_{\text{slope}} = 1/\tau_c$.

Appendix B

The semi-infinite solution of Green's function $g_1(r, \tau)$ can be simplified to exponential at the small delay-time. As shown
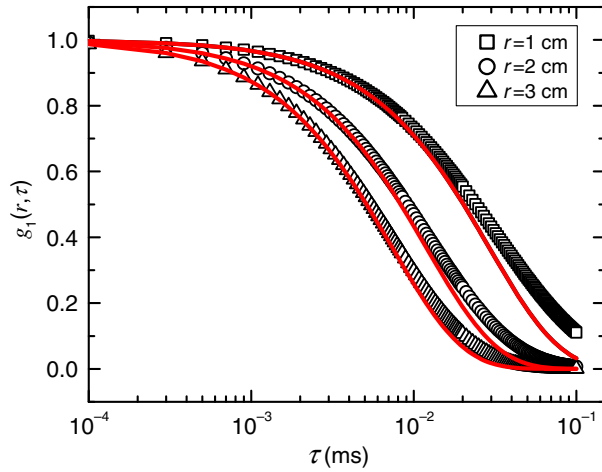
Fig. 10 Autocorrelation function $g_1(r, \tau)$ plotted as a function of the delay-time τ at different SD separations r. The red lines are calculated by Eq. (24). Here $n = 1.33$, $\beta = 1$, $\lambda = 671$ nm, $\mu_a = 0.1$ cm^{-1}, $\mu_s' = 10$ cm^{-1}, and $\alpha D_B = 2 \times 10^{-8}$ cm^2/s.

in Appendix A, the correlation function $G_1(r, \tau)$ can be written as

$$G_1(r, \tau)$$
$$= \frac{3\mu_s'}{4\pi} \frac{\exp[-K(\tau)r_1]}{r_1} \left\{ 1 - \exp\left[-\frac{K(\tau)z^2}{r_1} \right] \left(1 - \frac{z^2}{r_1^2} \right) \right\}.$$
(21)

When the time τ is small, Eq. (21) can be simplified to

$$G_1(r, \tau) \approx \frac{3\mu_s'}{4\pi} z^2 \frac{\exp[-K(\tau)r_1]}{r_1^2} \left[K(\tau) + \frac{1}{r_1} \right].$$
(22)

So the electric field autocorrelation function $g_1(r, \tau)$ at small delay-time can be simplified to

$$g_1(r, \tau) = \frac{G_1(r, \tau)}{G_1(r, 0)} \approx \exp\left(-\frac{Fr_1\tau}{2K_0} \right) \left[1 + \frac{Fr_1\tau}{2K_0(r_1K_0 + 1)} \right].$$
(23)

In the small delay-time $\exp\left[\frac{Fr_1\tau}{2K_0(r_1K_0+1)} \right] \approx 1 + \frac{Fr_1\tau}{2K_0(r_1K_0+1)}$, $g_1(r, \tau)$ can be further simplified to be exponential

$$g_1(r, \tau) \approx \exp\left[-\frac{Fr_1^2\tau}{2(r_1K_0 + 1)} \right].$$
(24)

We note that this simplified Eq. (24) is different from the result $g_1(r, \tau) \approx \exp(-Fr_1\tau/2K_0)$ in Ref. 48 which is obtained from Eq. (23) in a more stringent limit, i.e., $1 + Fr_1\tau/[2K_0(r_1K_0 + 1)] \approx 1$. This approximation $g_1(r, \tau) \approx \exp(-Fr_1\tau/2K_0)$ is valid only when the delay-time τ is very small. Our result of Eq. (24) can provide comparatively accurate approximation even in a larger range of delay-time as shown in Fig. 10.

Disclosures

No conflicts of interest, financial or otherwise, are declared by the authors.

References

1. A. Fercher and J. Briers, "Flow visualizaiton by means of single-exposure speckle photography," *Opt. Commun.* **37**(5), 326–330 (1981).
2. J. D. Briers and S. Webster, "Laser speckle contrast analysis (LASCA): a nonscanning, full-field technique for monitoring capillay blood flow," *J. Biomed. Opt.* **1**(2), 174–179 (1996).
3. D. A. Boas and A. K. Dunn, "Laser speckle contrast imaging in biomedical optics," *J. Biomed. Opt.* **15**(1), 011109 (2010).
4. D. Briers et al., "Laser speckle contrast imaging: theoretical and practical limitations," *J. Biomed. Opt.* **18**(6), 066018 (2013).
5. N. Hecht et al., "Intraoperative monitoring of cerebral blood flow by laser speckle contrast analysis," *Neurosurg. Focus* **27**(4), E11 (2009).
6. A. B. Parthasarathy et al., "Laser speckle contrast imaging of cerebral blood flow in human during neurosurgery: a pilot clinical study," *J. Biomed. Opt.* **15**(6), 066030 (2010).
7. E. Klijn et al., "Laser speckle imaging identification of increases in cortical microcirculatory blood flow induced by motor activity during awake craniotomy," *J. Neurosurg.* **118**(2), 280–286 (2013).
8. L. M. Richards et al., "Intraoperative laser speckle contrast imaging with retrospective motion correction for quantitative assessment of cerebral blood flow," *Neurophotonics* **1**(1), 015006 (2014).
9. W. J. Tom et al., "Efficient processing of laser speckle contrast images," *IEEE Trans. Med. Imaging* **27**(12), 1728–1738 (2008).
10. J. C. Ramirez-San-Juan et al., "Impact of velocity distribution assumption on simplified laser speckle imaging equation," *Opt. Express* **16**(5), 3197–3203 (2008).
11. B. J. Berne and R. Pecora, *Dynamic Light Scattering: With Applications to Chemistry, Biology, and Physics*, Dover Publications, Mineola, New York (2000).
12. R. Bonner and R. Nossal, "Model for laser Doppler measurements of blood flow in tissue," *Appl. Opt.* **20**(12), 2097–2107 (1981).
13. R. Bandyopadhyay et al., "Speckle-visibility spectorscopy: a tool to study time-varying dynamics," *Rev. Sci. Instrum.* **76**(9), 093110 (2005).
14. P. Zakharov et al., "Quantitative modeling of laser speckle imaging," *Opt. Lett.* **31**(23), 3465–3467 (2006).
15. A. B. Parthasarathy et al., "Robust flow measurement with multi-exposure speckle imaging," *Opt. Express* **16**(3), 1975–1989 (2008).
16. J. C. Ramirez-San-Juan et al., "Simple correlation factor for laser speckle imaging of flow dynamics," *Opt. Lett.* **39**(3), 678–681 (2014).
17. A. B. Parthasarathy et al., "Quantitative imaging of ischemic stroke through thinned skull in mice with multi exposure speckle imaging," *Biomed. Opt. Express* **1**(1), 246–259 (2010).
18. S. M. S. Kazmi et al., "Chronic imaging of cortical blood flow using multi-exposure speckle imaging," *J. Cereb. Blood Flow Metab.* **33**(6), 798–808 (2013).
19. D. D. Duncan and S. J. Kirkpatrick, "Can laser speckle flowmetry be made a quantitative tool," *J. Opt. Soc. Am. A* **25**(8), 2088–2094 (2008).
20. M. A. Davis et al., "Imaging depth and multiple scattering in laser speckle contrast imaging," *J. Biomed. Opt.* **19**(8), 086001 (2014).
21. S. M. S. Kazmi et al., "Flux or speed? Examining speckle contrast imaging of vascular flows," *Biomed. Opt. Express* **6**(7), 2588–2608 (2015).
22. D. A. Boas et al., "Scattering and imaging with diffusing temporal field correlations," *Phys. Rev. Lett.* **75**(9), 1855–1858 (1995).
23. D. A. Boas and A. G. Yodh, "Spatially varying dynamical properties of turbid media probed with diffusing temporal light correlation," *J. Opt. Soc. Am. A* **14**(1), 192–215 (1997).
24. R. Bi et al., "Deep tissue flowmetry based on diffuse speckle contrast analysis," *Opt. Lett.* **38**(9), 1401–1403 (2013).
25. R. Bi et al., "Multi-channel deep tissue flowmetry based on temporal diffuse speckle contrast analysis," *Opt. Express* **21**(19), 22854–22861 (2013).
26. D. Irwin et al., "Influences of tissue absorption and scattering on diffuse correlation spectroscopy blood flow measurements," *Biomed. Opt. Express* **2**(7), 1969–1985 (2011).

27. Z. Hajjarian and S. K. Nadkarni, "Correction of optical absorption and scattering variations in laser speckle rheology measurements," *Opt. Express* **22**(6), 6349–6361 (2014).
28. K. Khaksari and S. J. Kirkpatrick, "Combined effects of scattering and absorption on laser speckle contrast imaging," *J. Biomed. Opt.* **21**(7), 076002 (2016).
29. J. Liu et al., "Quantitatively assessing flow velocity by the slope of the inverse square of the contrast values versus camera exposure time," *Opt. Express* **22**(16), 19327–19336 (2014).
30. T. Durduran et al., "Diffuse optics for tissue monitoring and tomography," *Rep. Prog. Phys.* **73**(7), 076701 (2010).
31. S. A. Carp et al., "Due to intravascular multiple sequential scattering, diffuse correlation spectroscopy of tissue primarily measures relative red blood cell motion within vessels," *Biomed. Opt. Express* **2**(7), 2047–2054 (2011).
32. K. Verdecchia et al., "Assessment of the best flow model to characterize diffuse correlation spectroscopy data acquired directly on the brain," *Biomed. Opt. Express* **6**(11), 4288–4301 (2015).
33. A. Nadort et al., "Quantitative laser speckle flowmetry of the in vivo microcirculation using sidestream dark field microscopy," *Biomed. Opt. Express* **4**(11), 2347–2361 (2013).
34. R. C. Haskell et al., "Boundary conditions for the diffusion equation in radiative transfer," *J. Opt. Soc. Am. A* **11**(10), 2727–2741 (1994).
35. P.-A. Lemieux and D. J. Durian, "Investigating non-Gaussian scattering processes by using nth-order intensity correlation functions," *J. Opt. Soc. Am. A* **16**(7), 1651–1664 (1999).
36. C. P. Valdels et al., "Speckle contrast optical spectroscopy, a non-invasive, diffuse optical method for measuring microvascular blood flow in tissue," *Biomed. Opt. Express* **5**(8), 2769–2784 (2014).
37. H. M. Varma et al., "Speckle contrast optical tomography: a new method for deep tissue three-dimensional tomography of blood flow," *Biomed. Opt. Express* **5**(4), 1275–1289 (2014).
38. R. Michels et al., "Optical properties of fat emulsions," *Opt. Express* **16**(8), 5907–5925 (2008).
39. P. D. Ninni et al., "The use of India ink in tissue-simulating phantoms," *Opt. Express* **18**(26), 26854–26865 (2010).
40. G. Zaccanti et al., "Measurements of optical properties of high-density media," *Appl. Opt.* **42**(19), 4023–4030 (2003).
41. R. M. Pope and E. S. Fry, "Absorption spectrum (380–700 nm) of pure water. II. Integrating cavity measurements," *Appl. Opt.* **36**(33), 8710–8723 (1997).
42. S. Yuan, "Sensitivity, noise and quantitative model of laser speckle contrast imaging," Ph. D. Thesis, Tufts University (2008).
43. S. Yuan et al., "Determination of optimal exposure time for imaging of blood flow changes with laser speckle contrast imaging," *Appl. Opt.* **44**(10), 1823–1830 (2005).
44. S. M. S. Kazmi et al., "Optimization of camera exposure durations for multi exposure speckle imaging of the microcirculation," *Biomed. Opt. Express* **5**(7), 2157–2171 (2014).
45. C. Yeo et al., "Avian embryo monitoring during incubation using multi-channel diffuse speckle contrast analysis," *Biomed. Opt. Express* **7**(1), 93–98 (2016).
46. R. Bi et al., "Optical methods for blood perfusion measurement-theoretical comparison among four different modalities," *J. Opt. Soc. Am. A* **32**(5), 860–866 (2015).
47. M. Seong et al., "Simultaneous blood flow and blood oxygenation measurements using a combination of diffuse speckle contrast analysis and near-infrared spectroscopy," *J. Biomed. Opt.* **21**(2), 027001 (2016).
48. W. B. Baker et al., "Modified Beer–Lambert law for blood flow," *Biomed. Opt. Express* **5**(11), 4053–4075 (2014).

Jialin Liu received his BS degree in optical science and technology from Nanjing University of Science and Technology, Nanjing, China, in 2011. He is currently pursuing his PhD in optical engineering at Nanjing University of Science and Technology. His main research interests include laser speckle contrast imaging and image processing.

Hongchao Zhang is currently a lecturer of the School of Science, Nanjing University of Science and Technology. He is also a researcher of the Collaborative Innovation Center of Launch Technology, Nanjing University of Science and Technology. He received his PhD in instrumental science and technology from Nanjing University of Science and Technology in 2009. His research interests include interferometry of laser-induced plasma, image processing, and laser-induced damage.

Jian Lu is currently a professor of the School of Science, Nanjing University of Science and Technology, since 1996. He received his BS degree in physics from Nanjing Normal University, Nanjing, China, in 1985 and his PhD in applied physics from Nanjing University of Science and Technology, Nanjing, in 1995. His research interests include laser interaction with matter, optical imaging, and laser-induced damage.

Xiaowu Ni is currently a professor of the School of Science, Nanjing University of Science and Technology. He received his BS degree in applied physics from the East China Institute of technology, Nanjing, China, in 1978, his MS degree in applied physics from the East China Institute of Technology, in 1988, and his PhD in electronic engineering from the Southeast University, Nanjing, China, in 1997. His research interests include laser-induced damage, laser–bubble interaction, and laser interaction with biological tissue.

Zhonghua Shen is currently a professor of the School of Science, Nanjing University of Science and Technology. She received her BS degree in physics from Nanjing Normal University in 1994 and her PhD in optical engineering from Nanjing University of Science and Technology in 1999. She is also a postdoctor of the Institute of Acoustics, Nanjing University, from 1999 to 2001. Her research interests include laser ultrasonic, laser-induced damage, and laser interaction with biological tissue.